Land Mobile Propagation Satellite Model based on 360° images

Sébastien Rougerie, Jonathan Israel

Land Mobile Propagation Satellite Model based on 360° images

S. Rougerie[1] , J. Israel[2]
[1]CNES, Toulouse, France, Sebastien.Rougerie@cnes.fr
[2](ONERA): ONERA/DEMR, Université de Toulouse, France, jonathan.israel@onera.fr

***Abstract*— This paper presents a new concept of Land Mobile Propagation Satellite model. The main idea is to predict the propagation channel based on the analysis of 360° images. To do so, concurrent RF / optic measurements have been done in the past and this paper will present the correlation study between the images and RF signal. Finally, a coupling model RF / images is proposed here, which allows a LMS channel prediction between 1 to 30 GHz.**

***Index Terms*— LMS, RF signal, 1 – 30 GHz, images, deep learning processing**

I. INTRODUCTION

The knowledge of the Land Mobile Satellite (LMS) propagation channel is a key issue for the design of new satellite services at frequencies ranging from the L-band (GNSS) to the Ku-Ka band (SatCom). Therefore, based on physical and statistical considerations, several models have been developed and compared to measurements to assess the impact of the local environment of the receiver on the RF signal. The model ITU-R P681 Section 6 [3] proposes a statistical modeling of LMS channel. It is reliable for frequencies between 1 to 30 GHz, and for several environments (train, highway, sub-urban, wooded …).
This model has been built thanks to extensive measurements campaigns at L, S and C band ([4], [5], [6], [1]) and Ku, Ka band [7], [2]. This model provides reliable results for selected overall environments and frequencies, and can be used for receiver testing and link budget estimation. However, there are two intrinsic limitations: first, the model cannot reproduce the RF effect of a specific environment since it would need a 3D model of the environment, which is not an easy task. Moreover, the realization of such measurement campaigns is expensive due to the complexity of RF systems and to the expertise their use requires.
The use of low cost sensors such as fish-eye cameras is easy and provides rich information on the environment close to the receiver. Characterizing the LMS propagation channel thanks to optical analysis is therefore a cost-effective and complementary approach. This characterization has often been done following a two-state description resulting from the detection of the sky in the fish-eye images. For instance, [8] performs such a classification before estimating the satellite reception state as a line-of-sight (LOS) or a non-line-of-sight (NLOS) state. The resulting LOS / NLOS classification is consistent with measurements of Sirius XM Radio signals at 2.3 GHz, [9]. This approach has already been extended in order to refine the RF signal model by taking into account the driving direction [10] or the diffraction effects occurring in shadowed areas [11]. Fish-eye images have also been considered to characterize the receiver local environment in GNSS applications such as in [12] and [13], where texture and color cooccurence matrices are used to perform the image segmentation (sky, NLOS). In [15], the authors propose to use the fish-eye images to classify the local environment in four classes: Sky, Vegetation, poles or defoliated trees and other man-made structures such as buildings. For each class, the statistics associated to the RF signal (extracted from measurement, [1]) are provided and give a first idea of signal fading associated to each LOS and NLOS situation.
In this paper, the concept proposed in [15] is enhanced with two main improvements: first, the images processing is enhanced with the help of deep learning processing available in the literature (section II of the paper). Second, we propose a statistical model (similar as the one in ITU-R P681 Section 6) in order to link the images classification with the effect on the RF signal. This coupling model will be described in section III. The section IV will present the main validation results for several frequencies band (L, S C and Ka), and section V will present our conclusions.

II. IMAGES PROCESSING FOR CLOSE ENVIRONMENT CLASSIFICATION

Image classification and segmentation are very active and competitive research domains. Competitions are proposed each year, and deep learning based technics are among the most effective algorithms in several contests. The Table 1 present the main competition results for images segmentation / classification of the past years ([20]).

Table 1: Competition results for images classification / segmentation

Competition	Date/Deadline	Image size	Improvement	Winner
ICDAR 2011 Chinese handwriting	May 15, 2011	variable	3.8% / 28.9%	IDSIA [18e,19]
IJCNN 2011 traffic signs	Aug 02, 2011	variable	**68.0%**	IDSIA [18c-d,19]
ISBI 2012 brain segmentation	Mar 01, 2012	512x512	26.1%	IDSIA [20d,20d+]
ICPR 2012 cancer detection	Sep 10, 2012	2048x2048x3	8.9%	IDSIA [20a]
ImageNet 2012	Sep 30, 2012	256x256x3	41.4%	Univ. Toronto [19b]~[19]
MICCAI 2013 Grand Challenge	Sep 08, 2013	2048x2048x3	26.5%	IDSIA [20b,c]
ImageNet 2015	Sep 30, 2015	256x256x3	15.8%	Microsoft [12]~[11]

From them, we decided to use the FCN-8s (Fully Convolutional Networks) solution described in [18] in order to classify our images.

The first challenge in deep learning processing is to train the algorithms i.e. provide a reference database of images already classified. We remind that the target is here to classify the images in four classes: Sky, Vegetation, poles or defoliated trees and other man-made structures such as buildings. To do so, we investigate two available databases: the SYNTHIA database [16] and the CAMVID database [17]. Here, we meet the main issue of the deep learning approach as these datasets are very different from the images collected in [1] and [2]. The SYNTHIA dataset proposes realistic synthetic images, but the contrast is too important (the edges of objects are much too clear) and the color homogeneity of the objects is too high. Last, there is no dazzling effect due to the sun in the SYNTHIA dataset similar as what we may observe in our collected images (see for example Figure 2). The resolution and the size of the images available in the CAMVID datasets are very different from the ones we collected in [1] and [2] and thus, these images cannot be used for the algorithms training. Finally, we decided to train the deep learning algorithms with images extracted from our dataset. To do so, we adapted the *LabelImg* software [18] and we manually classified the pixels of the images as we can see in Figure 1. The selection of the images for the deep learning training is completely random, and around 100 images were selected and classified manually among more than 10 000 images.

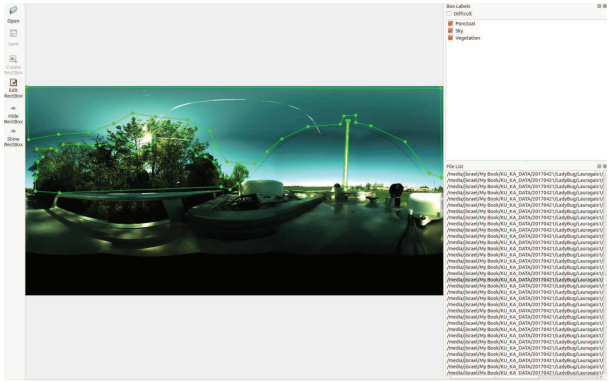

Figure 1: *LabelImgv* Software and an example of handmade image classification

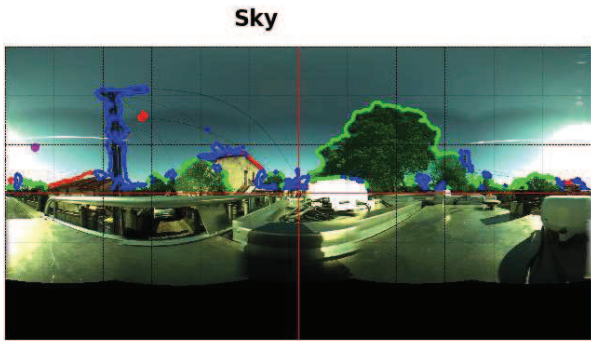

Figure 2: Processed image from [2] (Ka band measurement) in LOS situation

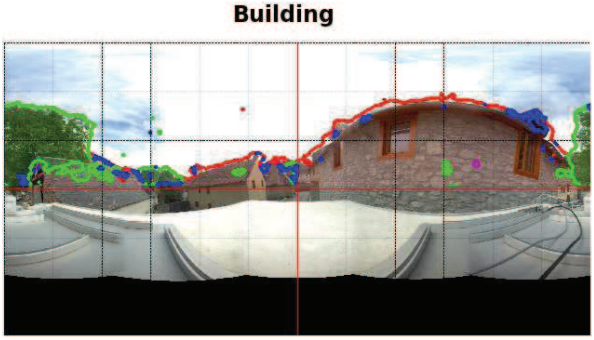

Figure 3: Processed image from [1] (S band measurement) in NLOS situation (here signal blocked by building)

After the algorithm training, Figure 2 and Figure 3 present the classification results of the deep learning algorithms respectively done on Ka band database [2] and S band database [1]. The green border represents pixels tagged as "vegetation", the red border the pixels tagged as "building", the blue border pixels tagged as "pole", and the whole other pixels are therefore tagged as "sky". With a visual inspection, the classification looks coherent. A global performance evaluation of the image classification process is under way and will be presented in the near future.

The magenta dot represents the satellite position, and thus we can associate the image classification with the signal power observed on the transmission as we can see in Figure 4. Then, we can propose a model which links the image classification with the RF attenuation and multipath power. This model is presented in the next section.

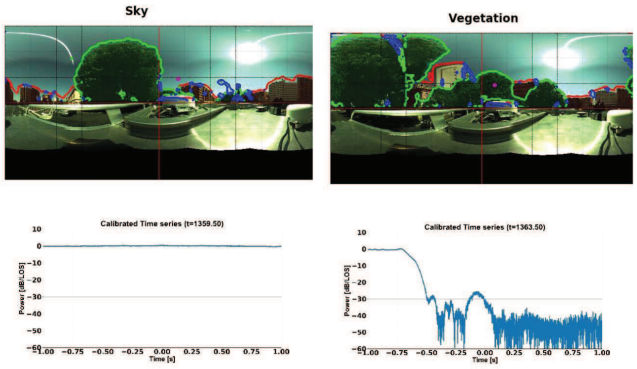

Figure 4: Deep learning classification vs signal power. LOS situation left, NLOS (signal bloc by vegetation) right

III. RF / IMAGES COUPLING MODEL

For the RF/images coupling mode, we propose to use the same approach as in ITU-R P681 [3]. In [3], the LMSS propagation environments can be rural, wooded, urban, suburban, and thus it is a mixture of different propagation conditions. The Cumulative Distribution Function (CDF) of signal levels in such mixed conditions is modelled by the enhanced 2-state semi-Markov model which is composed of a GOOD state, including slightly shadowed conditions, and a BAD state, including more severe shadowed conditions. The amplitude of the channel complex envelope in the Good and Bad states is modelled by a set of Loo distributions defined by the Loo triplet parameters (M_{Ai}, Σ_{Ai}, MP_i), respectively the mean of the direct signal, the standard deviation of the direct signal and the mean of the multipath.

$$p_{loo}(x) = \frac{x}{\Sigma_{Ai}\sigma_i^2\sqrt{2\pi}} \int_0^\infty \frac{1}{a} \exp\left[-\frac{(\ln(a) - M_{Ai})^2}{2\Sigma_{Ai}^2} - \frac{x^2 + a^2}{2\sigma_i^2}\right] I_0\left(\frac{xa}{\sigma_i^2}\right) da$$

The average direct path amplitude M_{Ai} is assumed to be normally distributed on a limited probability range, and the diffuse multipath component follows a Rayleigh distribution. The standard deviation of the direct path amplitude and the multipath power are linearly connected to the average direct path amplitude. Between a Good and Bad event, a stochastic transition length $L_{trans,i}$ is also introduced. Finally, the input parameters which have to be optimized for both the statistical and generative versions of the channel model are summarized in the Table 2.

The main idea here is to use the same approach, but the "Good" and "Bad" states will be substituted by the image classification: Sky, Vegetation, and buildings. For the pole, we will use an additional Kirchhoff diffraction model. Thus, the parameters to inverse are now given in Table 3.

Table 2: Input parameters in ITU-R P681 [3]

Parameter	Description
$(\mu,\sigma)_{G,B}$	Mean and standard deviation of the log-normal law assumed for events duration(meters)
$dur_{minG,B}$	Minimum possible events duration (meters)
$(\mu_{M_{A,GB}}, \sigma_{M_{A,GB}})$	Parameters of the $M_{A\ G,B}$ distribution, (M_A being the average value of the direct path amplitude A over one event (dB)
$MP = h_{1G,B}M_A + h_{2G,B}$	Multipath power, $MP_{G,B,}$ (one 1st order polynomial for each state), (dB)
$\Sigma_{A,\ GB} = g_{1G,B}M_A + g_{2G,B}$	Standard deviation of A, $\Sigma_{A,GB}$ (one 1st order polynomial for each state)
$L_{corrG,B}$*	Direct path amplitude correlation distance (meters)
$L_{trans,i} = f_1\Delta M_A + f_2$	Transition length, L_{trans} ,(one single 1st order polynomial), (meters)
$[p_{B,min}, p_{B,max}]$	Probability range to consider for the $M_{A\ B}$ distribution

Table 3: Input parameters in proposed RF / image model

Paramètres	Description
$(\mu,\sigma)_{sky}$ / $(\mu,\sigma)_{assembly}$ / $(\mu,\sigma)_{vegetation}$ (m)	Mean and standard deviation of the log-normal law assumed for for states *sky, assembly and* et *vegetation* (en m).
$(\mu_{MA},\sigma_{MA})_{sky}$ / $(\mu_{MA},\sigma_{MA})_{assembly}$ / $(\mu_{MA},\sigma_{MA})_{vegetation}$(dB)	Parameters of the M_{Ai}, for each image states (dB)
$g_{1,sky}M_A+g_{2,sky}$ / $g_{1,assembly}M_A+g_{2,assembly}$ / $g_{1,vegetation}M_A+g_{2,vegetation}$	Standard deviation of A for image states (dB)
$h_{1skyMA}+h_{2sky}$ / $h_{1assemblyMA}+h_{2assembly}$ / $h_{1vegetationMA}+h_{2vegetation}$	Multipath power for image states (dB)
$L_{corr\ sky,assembly,\ vegetation}$	Direct path amplitude correlation distance (m).
$f_1\Delta M_A+f_2$	Transition length for each images states
$dur_{min,sky}$ / $dur_{min,assembly}$ / $dur_{min,vegetation}$	Minimum possible events duration (meters)

To retrieve the model parameters, we used the same methodology as in the ITU-R P681 (the parameters inversion is described in the fascicle [3]). There are only two differences: first, we do not need to make a state identification based on fuzzy logic here as the states are now given by the image classification. Second, instead of having two states, we have now 3 classifications. Based on the measurement done in [1] (S and C band) and [2] (Ka band), we were able to inverse the parameters for several frequencies. In Table 4, we present the retrieved parameters for S, C and Ka band, associated to a sub-urban environment.

Table 4: Retrieve parameters for RF / image model

Parameters	S band	C band	Ka band
$(\mu,\sigma)_{sky}$ / $(\mu,\sigma)_{assembly}$ / $(\mu,\sigma)_{vegetation}$	(0.64, 1.61) / (1.66, 1.42) / (1.76, 1.38)	(1.07, 1.47) / (1.39, 1.31) / (1.67, 1.31)	(2.36, 1.55) / (0.46, 1.34) / (0.05, 1.30)
$(\mu_{MA},\sigma_{MA})_{sky}$ /	0.10 / 0.10 / 0.50	0.10 / 0.10 / 0.50	0.01 / 0.50 / 0.50

$(\mu_{MA},\sigma_{MA})_{assembly}$ / $(\mu_{MA},\sigma_{MA})_{vegetation}$ (dB)			
$g_{1,sky}M_A+g_{2,sky}$ / $g_{1,assembly}M_A+g_{2,assembly}$ / $g_{1,vegetation}M_A+g_{2,vegetation}$	(-0.12, 1.13) / (-9.33, 7.92) / (-7.62, 7.65)	(-8.56, 8.82) / (-6.19, 7.98)	(-0.28, 0.56) / (-6.21, 8.63) / (-9.82, 8.14)
$h_{1skyMA}+h_{2sky}$ / $h_{1assemblyMA}+h_{2assembly}$ / $h_{1vegetationMA}+h_{2vegetation}$	(-0.12, 1.13) / (-0.39, 0.00) / (-0.38, 0.00)	(0.16, 1.12) / (-0.33, 0.00) / (-0.35, 0.00)	(-0.28, 0.56) / (-0.23, 0.00) / (-0.52, 0.00)
$L_{corr\ sky,assembly,vegetation}$	(0.00, -15.23) / (0.45, -11.55) / (0.47, -11.69)	(0.00, -16.28) / (0.49, -12.87) / (0.48, -12.95)	(0.00, -26.36) / (0.51, -20.58) / (0.22, -19.58)
$f_1\Delta M_A+f_2$	0.50	0.50	0.50
$dur_{min,sky}$ / $dur_{min,assembly}$ / $dur_{min,vegetation}$	0.04 / 3.00	0.04 / 3.00	0.04 / 3.00

IV. MODEL VALIDATION

To validate the proposed model, we compare the experimental and generated time series CDF and the fade duration CDF. In Figure 5, Figure 6 and Figure 7, we plot these CDF respectively for S, C (from data base [1]) and Ka band (from data base [2]). As we can see, the experimental and modeled curves fit quite well.

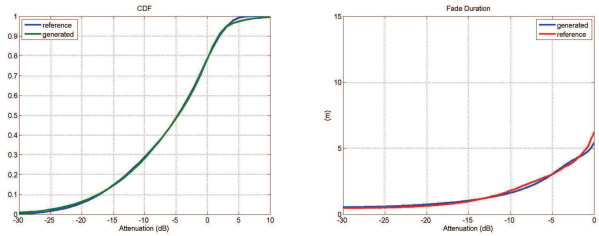

Figure 5: time series CDF and fade duration CDF, S band. Model vs data [1]

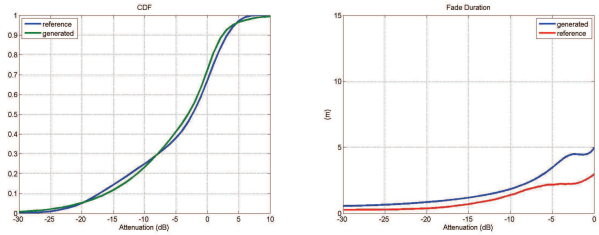

Figure 6: time series CDF and fade duration CDF, C band. Model vs data [1]

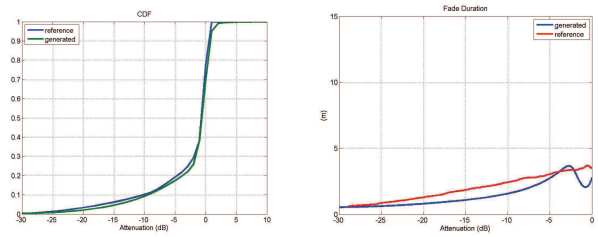

Figure 7: Time series CDF and fade duration CDF, Ka band model vs data [2]

In [3], some guidelines are given in order to evaluate the fit performances. The acceptance criteria are on the Root Mean Square of absolute difference of fading margin (Err_FM), Average fade duration (Err_AFD) and Rice factor (Err_K). The input parameters are accepted if Err_FM $\leq$ 2dB, Err_AFD $\leq$ 1 m and Err_K $\leq$ resolution_K (Synthetic Rice factor series computed applying the Method of Moments on the fading synthetic series). For each frequency band, the inversion criteria are given in Table 5, and we can see that all the values are under the acceptable threshold. Thus, the proposed model is validated.

Table 5: Performance inversion criteria

Erreur RMS	S band	C band	Ka band
Err_FM (dB) < 2dB	0.64	1.11	0.66
Err_AFD (m) < 1 m	0.15	0.72	0.64
K factor < Resolution	0.61 | 4.68	0.62 | 5.17	5.17 | 5.76

V. CONCLUSIONS

This paper presents a model in order to extrapolate, from 360° images, the land mobile satellite channel. Two main components are part of this model: first, an image processing tool based on deep learning solution is used in order to classify the image's pixels in 4 states: sky, Vegetation, pole and building. Second, a statistical model, inspired from the ITU-R P681 model, proposes to link the images states with the propagation channel (fading and multipath rice factor). At the end, it is possible with this tool to provide an estimation of the propagation condition based only on images.

In the future work, we will investigate if we can couple the image states detection with a physical / statistical channel model such as the SCHUN simulator [19] for L to C band, or the CNES / ONERA Ka band simulator.

REFERENCES

[1] M. Ait-Ighil, T. Deloues, J. Lemorton, F. Issac, S. Rougerie, « Doppler Spectrum Measurements for Land Mobile Satellite Systems Around 2.2 GHz and 3.8 GHz", EUCAP 2016, Davos

[2] S. Rougerie, B. Benammar, "Concurent Ka band RF measurement and sifh-eye Images for Land Mobile Satellite Propagation Channel", EUCAP 2018, London

[3] Recommendation ITU-R P.681-11, “Propagation data required for design systems in the land mobile-satellite service”, 08/2019.

[4] G.Carrié, F.Perez Fontan, F.Lacoste, J.Lemorton, “A Generative MIMO Channel Model Encompassing Single Satellite and Satellite Diversity Cases”, ESA workshop on radiowave propagation, Noordwijk, NL, November 2011

[5] B.Montenegro Villacieros, “Versatile Two State Model For Land Mobile Satellite Systems: Parameter Extraction And Time Series Synthesis”, PhD Thesis, UCL, Belgium, Sep. 2011

[6] D. Arndt, T. Heyn, R. Prieto-Cerdeira, E. Eberlein, “Extended Two-State Narrowband LMS Propagation Model for S-Band”, IEEE BMSB symposium, Seoul, Korea, June 2012

[7] T. Heyn, E. Eberlein, D. Arndt, B. Matuz, F. Lázaro Blasco, R. Prieto-Cerdeira, J. Rivera-Castro, “Mobile Satellite Channel with Angle Diversity: the MiLADY Project”, EuCAP conference, Barcelona, April 2010

[8] M. Rieche, D. Arndt, A. Ihlow, and G. D. Galdo, “State modeling of the land mobile satellite channel by an image-based approach,” in 2013 7th European Conference on Antennas and Propagation (EuCAP), Apr. 2013, pp. 672–676.

[9] A. Ihlow, D. Arndt, F. Topf, C. Rothaug, T. Wittenberg, and A. Heuberger, “Photogrammetric satellite service prediction – Correlation of RF measurements and image data,” in 2011 IEEE International Symposium on Broadband Multimedia Systems and Broadcasting (BMSB), Jun. 2011, pp. 1–6

[10] M. Rieche, D. Arndt, A. Ihlow, F. Prez-Fontn, and G. D. Galdo, “Impact of driving direction on Land Mobile Satellite channel modeling,” in The 8th European Conference on Antennas and Propagation (EuCAP 2014), Apr. 2014, pp. 2268–2271.

[11] M. Rieche, A. Ihlow, T. Heyn, F. Prez-Fontn, and G. D. Galdo, “Land mobile satellite propagation characteristics from knife-edge diffraction modeling and hemispheric images,” in 2015 9th European Conference on Antennas and Propagation (EuCAP), May 2015, pp. 1–4

[12] A. Cohen, C. Meurie, Y. Ruichek, and J. Marais, “Characterization of the reception environment of GNSS signals using a texture and color based adaptive segmentation technique,” in 2010 IEEE Intelligent Vehicles Symposium, Jun. 2010, pp. 275–280.

[13] A Cohen, C. Meurie, Y. Ruichek, J. Marais, and A. Flancquart, “Quantification of GNSS signals accuracy: An image segmentation method for estimating the percentage of sky,” in 2009 IEEE International Conference on Vehicular Electronics and Safety (ICVES), Nov. 2009, pp. 35–40.

[14] D. Attia, C. Meurie, Y. Ruichek, and J. Marais, “Counting of satellites with direct GNSS signals using Fisheye camera: A comparison of clustering algorithms,” in 2011 14th International IEEE Conference on Intelligent Transportation Systems (ITSC), Oct. 2011, pp. 7–12.

[15] J. Israel, M. Ait Ighil, “Land Mobile Satellite Propagation Channel Characterization Based On RF Measurements And Fish-eye Images”. VTC Fall 2017

[16] SYNTHIA dataset, http://synthia-dataset.net/

[17] CAMVID dataset, http://mi.eng.cam.ac.uk/research/projects/VideoRec/CamVid/

[18] J. Long, E. Shelhamer and T. Darrell, "Fully convolutional networks for semantic segmentation," *2015 IEEE Conference on Computer Vision and Pattern Recognition (CVPR)*, Boston, MA, 2015, pp. 3431-3440.*https://github.com/tzutalin/labelImg*Appendix to the ITU-R P 681, New fascicle on “Guidelines for parameter extraction and testing of Land Mobile Satellite narrowband channel models

[19] M. Ait Ighil, Hybrid Land Mobile Satellite Channel Simulator Enhanced for Multipath Modelling Applied to Satellite Navigation Systems”, PhD dissertation, 2012

[20] http://people.idsia.ch/~juergen/computer-vision-contests-won-by-gpu-cnns.html